The *Arabidopsis* Diacylglycerol Kinase 4 is involved in nitric oxide-dependent pollen tube guidance and fertilization

Authors

Aloysius Wong[1,2], Lara Donaldson[2,3], Maria Teresa Portes[4], Jörg Eppinger[5], José Feijó[4,*], Christoph Gehring[2]

Affiliations

[1] Department of Biology, College of Science and Technology, Wenzhou-Kean University, 88 Daxue Road, Ouhai, Wenzhou, Zhejiang Province, 325060, China

[2] Division of Biological and Environmental Sciences and Engineering, 4700 King Abdullah University of Science and Technology, Thuwal 23955-6900, Saudi Arabia

[3] Department of Molecular and Cell Biology, University of Cape Town, Rondebosch 7701, South Africa

[4] Department of Cell Biology and Molecular Genetics, University of Maryland, College Park, MD 20742-5815, USA

[5] Division of Physical Sciences and Engineering, Biological & Organometallic Catalysis Laboratory, KAUST Catalysis Center, 4700 King Abdullah University of Science and Technology, Thuwal 23955-6900, Saudi Arabia

* To whom correspondence should be addressed: jfeijo@umd.edu

Key words

DGK4; Pollen tube; Nitric oxide; Fertilization; Plant sexual reproduction; H-NOX; *Arabidopsis*

Abstract

Nitric oxide (NO) is a key signaling molecule that regulates diverse biological processes in both animals and plants including important roles in male gamete physiology. In plants, NO is generated in pollen tubes (PTs) and affects intracellular responses through the modulation of Ca^{2+} signaling, actin organization, vesicle trafficking and cell wall deposition bearing consequences in pollen-stigma interactions and PT guidance. In contrast, the NO-responsive proteins that mediate these responses remains elusive. Here we show that PTs of *Arabidopsis thaliana* impaired in the pollen-specific Diacylglycerol Kinase 4 (DGK4) grow slower and become insensitive to NO-dependent growth inhibition and re-orientation responses. Recombinant DGK4 protein yields NO-responsive spectral and catalytic changes *in vitro* which are compatible with a role in NO perception and signaling in PTs. In addition to the expected phosphatidic acid producing kinase activity, DGK4 recombinant protein also revealed guanylyl cyclase activity as hinted by sequence analysis. Our results are compatible with a role for the fast-diffusible NO gas in signaling and cell-cell communication via the modulation of DGK4 activity during the progamic phase of angiosperm reproduction.

Main Text

Introduction

Nitric oxide (NO) is a key signaling molecule that regulates diverse biological processes in animals and plants (Wendehenne et al., 2001; Lamattina et al., 2003). In animals, NO regulates vascular wall tone, neurotransmission and immune response while in plants, NO is essential for development and responses to biotic and abiotic stresses (Wendehenne et al., 2001; Domingos et al., 2015; Astier et al., 2019). Interestingly, NO is involved in the sexual reproduction of both animals and plants mediating events related to the male gamete physiology. In animals, NO stimulates sperm motility (Miraglia et al., 2011) and binding to the plasma membrane of oocytes (Sengoku et al., 1998), while in plants NO mediates pollen-stigma interactions and pollen tube (PT) guidance (McInnis et al., 2006; Prado et al., 2008). NO generation in PTs has been demonstrated (Prado et al., 2004) and intracellular responses to NO include modulation of cytosolic Ca^{2+} elevation (likely causal for PT growth retardation, re-orientation and re-growth), actin organization, vesicle trafficking and cell wall deposition (Prado et al., 2008; Wang et al., 2009). However, the NO-responsive proteins that mediate these responses remain unknown (Domingos et al. 2015; Leon and Costa-Broseta, 2019).

Previously, the pollen-specific *Arabidopsis* Diacylglycerol Kinase 4 (*DGK4*) (TAIR ID: At5g57690) has been suggested to harbor a gas-sensing region (Wong et al., 2013; Domingos et al., 2015) and the *DGK* family has been associated with important roles in pollen germination and growth (Potocký et al., 2014). Recently, *DGK4* has been

assigned signaling roles related to maintaining mechanical properties in PT growth with consequences on fertility rates (Dias et al., 2019).

Here we investigated the NO-dependent PT growth responses in wild-type (WT) (ecotype *Col-0*) and DGK4-impaired plants. We show that PTs of *Arabidopsis* impaired in the pollen-specific DGK4 grow slower and become partially insensitive to NO-dependent growth inhibition and re-orientation responses. Recombinant DGK4 yields NO-responsive spectral and catalytic changes *in vitro* which are compatible with a NO perception and signaling function in PTs. These results are discussed in the context of a role for NO, as a fast-diffusible gas, in DGK4-mediated long range signaling and/or rapid cell-cell communication during angiosperm reproduction.

Materials and Methods

Plant materials and growth conditions

Two mutant Arabidopsis lines (SALK_151239 and SALK_145081) with T-DNA insertions at the promoter of *DGK4* were obtained from the Nottingham Arabidopsis Stock Center (NASC) and progenies were PCR screened for homozygosity of mutant (T-DNA + *DGK4* reverse primer) and wild-type (*DGK4* promoter forward + *DGK4* reverse primer) chromosomes (Table S2). The homozygous mutant alleles were subsequently referred to as *dgk4-1* and *dgk4-2* respectively. The T-DNA insertion sites were confirmed by sequencing (KAUST Bioscience Core Lab, Saudi Arabia). All seeds were cold stratified at 4 °C for 3 days. *Col-0* wildtype and mutant lines were grown on soil (Jiffy, USA) containing 50% (w/v) of vermiculite in Percival growth chambers (CLF

89 Plant Climatics, Germany) at 22 ± 2 °C and 60% of relative humidity under long day (16
90 hours light) photoperiod (100 µM photons m^{-2} s^{-1}).
91
92 **Characterization of *dgk4* mutant plants**
93 RNA was extracted from pollen from approximately 300 flowers of WT and *dgk4-*
94 *1* mutants (Qiagen, USA) and cDNA synthesized using SuperScript III reverse
95 transcriptase according to manufacturer's instructions (Invitrogen, UK). The cDNA was
96 subjected to semi-quantitative RT-PCR with *DGK4* gene specific primers (Table S2) on
97 an AB thermal cycler (Bio-Rad, USA) and *DGK4* gene expression was normalized
98 against that of protein phosphatase 2A subunit A3, *PP2AA3* (At1g13320) (Table S2)
99 using the ImageLab software (Bio-Rad, USA).
100
101 ***In vitro* pollen germination**
102 *In vitro* pollen germination was performed as detailed previously (Prado et al., 2004;
103 Prado et al., 2008), but with optimized germination medium for *Arabidopsis* (Boavida
104 and McCormick, 2007) with or without the NO sources sodium nitroprusside (SNP) or
105 Diethylamine (DEA) NONOate. The growth of at least 100 PTs were measured on a
106 Nikon Eclipse TE2000-S inverted microscope equipped with an Andor iXon3 camera
107 across a range of pH (pH 6.5-8.5) and in optimal (5 mM) and low (100 µM) Ca^{2+} media.
108 In NO-treated pollen germination and PT growth experiments, at least 150 unique pollen
109 or PTs were considered. Image frames covering the entire growth area of the culture
110 dish that is mounted on automated stage, were acquired using the Nikon Eclipse
111 TE2000-S inverted microscope which is equipped with a Hamamatsu Flash28s CMOS

112 camera. The PT lengths were measured using NeuronJ (Meijering et al., 2004). For PT
113 re-orientation studies, PTs were challenged with a NO artificial point source by loading
114 by a glass micropipettes (OD 1.5mm, ID 1.2 mm, WPI) pulled to a tip with a ~ 5 µm
115 aperture filled with 10 mM SNAP (s-nitroso-acethilpenilcilamine) on agarified (1%)
116 germination medium. Typically, the pipette tip was placed 60 µm away from the growing
117 PT tip using a nanometer-stepper, motor-driven, three-dimensional positioner
118 (ScienceWares.com). Growth and bending response of growing PTs were monitored by
119 imaging using a Nikon Eclipse TE2000-S inverted microscope (PlanApo 40x, NA 1.3)
120 equipped with an Andor iXon3 camera and the bending angles measured using ImageJ
121 (Schneider et al., 2012).

122

123 **PT growth *in planta***

124 PT growth in the pistil of hand pollinated WT and *dgk4-1* plants was examined by
125 collecting the pistils at different time points (3-8 hours) after pollination. Aniline blue
126 staining of PTs in the pistil was performed as described previously (Mori et al., 2006)
127 and PT length in the pistil was measured using ImageJ (Schneider et al., 2012).

128

129 **Reproductive fitness test**

130 The reproductive fitness of *dgk4-1* was examined by crossing emasculated WT
131 (ecotype *Col-0*) flowers with pollen from both WT and *dgk4-1*. In detail, a ~50:50 mixture
132 of pollen from *Col-0* (*r/r*) and *dgk4-1* (*R/R*) was brushed onto an emasculated *Col-0*
133 flower (where *R* = resistant and *r* = susceptible), where pollen was effectively *R/r*
134 crossed onto the *Col-0* female (*r/r*). If there was no bias in fitness, then there should be

a 50% kanamycin resistant and 50% susceptible phenotype. If the *Col-0* pollen is fitter, then less than half of the offspring will be kanamycin resistant. The desiccated seeds were collected, surface sterilized and stored at 4 °C for 3 days before growing on MS agar (1.1% w/v) containing 100 µg/mL kanamycin (Sigma-Aldrich, St. Louis, MO). The proportion of WT to *dgk4-1* seeds were scored after 7 days of growth ($n > 70$).

Protein expression and purification

A Gateway compatible clone (DKLAT5G57690.1) containing the full-length coding sequence of *DGK4* was purchased from Arabidopsis Biological Resource Center (ABRC). The DGK4 sequence was recombined into the pDEST17 His-tagged expression vector and transformed into *E. coli BL21 A1* (Invitrogen, USA). Expression of recombinant DGK4 was induced with 0.2% (w/v) L-arabinose. Cells were lysed in a guanidium lysis buffer and the supernatant loaded onto a Ni-NTA agarose column for affinity purification under denaturing conditions using urea-containing buffers. Denatured recombinant DGK4 was re-folded by gradual dilution of urea in a linear gradient using an AKTA FPLC (GE Healthcare, UK). Hemin (30 µg/mL) was added to the re-folding buffers to allow for incorporation of heme into DGK4 as it assumes native conformation. Excess hemin was removed by size exclusion and recombinant DGK4 stored in 'Buffer' containing 20 mM $Na_2H_2PO_4$, 500 mM NaCl, 500 mM sucrose, 100 mM non-detergent sulfobetaines (NDSB), 0.05% (w/v) polyethylene glycol (PEG), 4 mM reduced glutathione, 0.04 mM oxidized glutathione and SIGMAFAST protease inhibitor cocktail (1 tablet per 100 mL solution).

Two single dgk4 mutants (H350L and Y379L) were constructed using site directed mutagenesis by PCR (Ho et al., 1989). To construct the H350L dgk4 mutant, two overlapping fragments of the DGK4 coding sequence both incorporating the mutation, were amplified from the pDEST17-*DGK4* plasmid using the respective *DGK4* F and *DGK4* H-L R (for 1st fragment amplification), and *DGK4* H-L F and *DGK4* R (for 2nd fragment amplification) primer pairs (Table S2). The two overlapping fragments both incorporating the mutations were then used as templates for a PCR reaction using the full-length *DGK4* F and *DGK4* R primer pairs (Table S2) which generated a full-length dgk4 H350L mutant sequence. The dgk4 Y379L mutant was generated using the same method but with the following mutagenic primers pairs, *DGK4* F and *DGK4* Y-L R, and *DGK4* Y-L F and *DGK4* R (Table S2). The *DGK4* mutant PCR products were inserted into the PCR8/GW/TOPO vector (Invitrogen, USA) by TA cloning, recombined into the pDEST17 His-tagged expression vector and transformed into *E. coli BL21 A1* (Invitrogen, USA). Mutant dgk4 was expressed and affinity purified in the same manner as DGK4.

UV-visible absorption spectroscopy

The UV-visible spectra of affinity purified recombinant DGK4 (200 µg/mL) was recorded on a PHERAstar FS micro-plate reader (BMG Labtech, USA). The heme environment of DGK4 was characterized by the addition of a reducing agent, sodium dithionite ($Na_2S_2O_4$) to a final concentration of 10 mM and absorbance was immediately measured and examined for spectral changes. The protein sample was then exposed to air and any recovery of the oxidized peak was monitored by the same spectra

measurements at 5 min intervals. The heme-NO complex was generated by immediately adding the NO donor DEA NONOate to a pre-reduced recombinant DGK4 before making the same spectral measurements.

DAG kinase and GC assays

DAG kinase assay and phospholipid extraction was performed using 30 µg purified recombinant protein in a reaction mixture containing 40 mM Bis-Tris (pH 7.5), 5 mM $MgCl_2$, 0.1 mM EDTA, 1 mM spermine, 0.5 mM dithiothreitol, 1 mM sodium deoxycholate, 0.02% (v/v) Triton X-100, 500 µM 1,2-DOG and 1 mM ATP, in the absence or presence of 1 mM SNP or 0.65 mM DEA NONOate. PA generated from the reactions was measured using the Total Phosphatidic Acid Assay kit according to the manufacturer's instructions (Cayman Chemical, Michigan USA).

GC assay was performed using 10 µg purified recombinant protein in a reaction mixture containing 50 mM Tris-HCl (pH 7.5), 1 mM GTP, 5 mM $MgCl_2$ or $MnCl_2$, in the absence or presence of 1 mM SNP or 0.65 mM DEA NONOate. cGMP generated from the reactions was measured using the cGMP enzyme immunoassay (EIA) Biotrak System with the acetylation protocol according to the manufacturer's instructions (GE Healthcare, Illinois USA).

Chemicals and statistical analysis

All chemicals were purchased from Sigma unless stated otherwise. Statistical analyses were performed using Student's *t*-test. Significance was set to a threshold of $P < 0.05$ and *n* values represent number of biological replicates.

Results and Discussion

DGK4 is required for NO-dependent PT growth and re-orientation responses

Homozygous *dgk4* plants with a T-DNA insertion 424 bp upstream of the *DGK4* ORF (*dgk4-1*; SALK_151239) were determined to have a 50% knockdown (KD) in *DGK4* expression (Figure S1). *dgk4-1* PTs grow significantly slower *in vitro* compared to WT across a pH range of 6.5-8.5 and in both optimal and reduced Ca^{2+} media (Figure 1A). After four hours of germination, WT PTs reached an average length of 176 µm while *dgk4-1* only reached 144 µm at pH 7.5 ($n > 100$; $P < 0.05$). This mutant line was also reported to have PTs with altered stiffness and adhesion properties (Dias et al., 2019). When exposed to the NO donor sodium nitroprusside (SNP), both WT and the *dgk4-1* PTs show NO dose-dependent reduction of growth rates (Figure 1B) much like those reported in *Lilium longiflorum* (Prado et al., 2004), *Paulownia tomentosa* (He et al., 2007) and *Camelia sinensis* (Wang et al., 2012). Between 0-10 nM of SNP, the decline in growth rate for WT is 34.52% but, in contrast, the decline for *dgk4-1* in the same range is only 7.86%. Importantly, PTs of *dgk4-1* become insensitive to SNP concentration increases over 50 nM while the rate of WT PT growth continues to decrease up to 200 nM SNP (Figures 1B and 1C). Correspondingly, we also observed differential sensitivity between WT and *dgk4-1* PTs using another NO donor, DEA NONOate (Figure 1B). A second independent homozygous *dgk4* mutant plant (*dgk4-2*; SALK_145081, T-DNA insertion 268 bp upstream of the *DGK4* gene) (Figure S1) showed similar NO insensitivity (Figure S2). These results suggest that the effect of NO on DGK4 activity has mechanistic consequences on PT growth.

We further examined the effect of NO on directional growth of PTs using *dgk4-1*. Our experimental set-up was based on our previous work in lily PTs (Prado et al., 2004) where an agarified medium containing 10 mM SNAP (s-nitroso-acethilpenilcilamine; NO donor) was loaded into a pulled glass micropipette, forming a point source of NO diffusion. Assuming that the germination medium is homogenous, a gradient concentration decrease with the square of the distance should be formed. For lily PTs, we experimentally determined that the threshold for the negative chemotropic re-orientation response was within the range of 5-10 nM of NO (Prado et al., 2004). Here, we reproduced these experiments with *Arabidopsis.* Both WT and *dgk-4* PTs were chosen to have growth rates within a similar range (2-4 $\mu m.min^{-1}$) to minimize growth rates bias to their NO response. We observed that WT and *dgk4-1* PTs showed a negative chemotropic response, bending away from the NO source much like our previous observations in lily (Prado et al., 2004), but, of relevance, the bending angles in WT (45.8 ± 6.3º; *n* = 10) were twice as sharp as those in *dgk4-1* (22.9 ± 2.6º; *n* = 10) (Figure 1D, Figure S3). Moreover, WT PTs showed clear, elbow-like, points of inflections when approaching the critical NO concentration, a morphological feature, also observed in lily (Prado et al., 2004) that corresponds to a slowdown of the growth rate, followed by turning of the PT (Movie S1). In contrast, *dgk4-1* PTs showed softer angles without elbow-like turns (Figure 1D) even when challenged with much steeper and concentrated gradients of SNAP (Figure S3). Both the germination and the re-orientation experiments clearly show a de-sensitization to NO, an effect that would be expected to be more pronounced if a full knock-out of *dgk4-1* would be available. Given

that a dose of 5-10 nM is within the physiological range of NO action (Lamattina et al., 2003), our results are consistent with a signaling role for DGK4 in NO sensing.

In agreement with the *in vitro* germination phenotype, *in vivo* germinated PTs of *dgk4-1* also grew slower down the pistil than those of WT across all time points examined (Figures 1E and 1F). To test if these differential growth rates would result in out-competition, we brushed a ~50:50 mixture of pollen from *Col-0* (*r/r*) and *dgk4-1* (*R/R*) onto an emasculated *Col-0* flower (where *R* = resistant and *r* = susceptible), generating a *R/r* pollen cross onto *Col-0* female (*r/r*). With no bias in fitness, a 1:1 ratio of kanamycin resistant and susceptible offspring would be expected, but rather we observed a ratio of 36.3% (*n* = 99) kanamycin resistant, revealing that WT PTs out-performed *dgk4-1* PTs. This finding is consistent with that reported for a different *dgk4* mutant allele (Dias et al., 2019).

DGK4 yields NO-responsive spectral changes and catalytic activity

We then focused on determining the molecular basis of the NO-sensing properties of DGK4. Through sequence analysis we have previously predicted that DGK4 contains a region spanning from H350 to R383 similar to heme centers of functional gas-responsive heme-NO/oxygen (H-NOX), heme-NO-binding and NO-sensing families of proteins in other kingdoms (Domingos et al., 2015; Wong et al., 2018). In particular, this region harbors the HX[12]PX[14,16]YXSXR consensus pattern derived for heme *b* containing H-NOX centers in proteins from bacteria and animals and, is present in plant orthologs such as poplar, castor bean and soybean but absent in other *Arabidopsis* DGKs (Figure 2A). The presence of the H-NOX-like signature

suggests that DGK4 may accommodate a heme *b* and correspondingly, the diagnostic spectral properties should have a distinct response to NO. Recombinant DGK4 yields a Soret peak at 410 nm (Figure 2B), which is distinctly different from unbound hemin (protohemine IX: Soret band at 435 nm with a shoulder at 400 nm) and falls within the typical peak range observed for proteins with a histidine-ligated ferric heme *b* (Walker et al., 1999). Reduction with sodium dithionite resulted in a red shift of the Soret peak to 424 nm accompanied by the emergence of distinct α (558 nm) and β (526 nm) bands (Figures 2B and S4A). The ferrous state presumably represents the native state of DGK4 in the cytosol (*A. thaliana* cytosolic redox potential: -310 to -240 mV (Aller et al., 2013)). Exposure to air recovers the oxidized Soret peak (410 nm) of DGK4 after 20 min (Figure S4A). Importantly, addition of DEA NONOate attenuates the reduced Soret absorption (424 nm) in a concentration dependent manner hinting at the possibility of NO displacing the histidine ligand from the heme group (Figures 2C and S4B). This is an essential step in the signaling of canonical H-NOX proteins (Russwurm and Koesling, 2004).

Qualitatively, the spectroscopic behavior resembles that of canonical H-NOX proteins e.g., the H-NOX domain of *S. oneidensis* which showed Soret absorptions at 403 nm (ferric), 430 nm (ferrous) and 399 nm (ferrous, NO-bound) (Dai et al., 2012). However, the frequencies and relative intensities of the Soret α and β peaks are indicative of a bis-histidine ligated heme *b* center as that found in cytochromes *b5* or a heme-based cis-trans carotene isomerase Z-ISO (Beltran et al., 2015). In accordance, DGK4 mutants which affect the heme binding site should produce a reduced heme absorption spectrum, as demonstrated for Z-ISO (Beltran et al., 2015). Indeed, H350L

and Y379L dgk4 mutants showed reduced Soret band intensities of about 50% and 70% respectively (Figure 2D). Since the Soret bands were still present in the mutants albeit attenuated, we can expect a similar behavior in their reductions and NO spectra which we did observe with the H350L mutant protein (Figure S4). Overall, the H350L dgk4 mutant recorded a much larger decrease in reduced Soret bands than that observed with DGK4 WT at low NO donor concentration (0.25 mM DEA NONOate) while also requiring a slightly longer time (~ 5 min more than DGK4 WT) to recover its oxidized Soret peak (410 nm) when exposed to air (Figure S4). Together with a marked reduction in Soret band intensities of dgk4 mutants, these results can be interpreted as a weakening of the heme environment. Our data are consistent with a recently identified *Arabidopsis* protein (AtLRB3; TAIR ID: At4g01160) harboring a H-NOX-like center, that yields canonical spectroscopic behavior of H-NOX proteins and for which mutation of the heme iron-coordinating histidine impaired the NO-response, like *dgk4* (Zarban et al., 2019).

Based on protein sequence analysis we previously predicted DGK4 to be a bifunctional catalytic protein with a canonical kinase domain capable of converting *sn*-1,2-diacylglycerol (DAG) with ATP into the corresponding phosphatidic acid (PA), but, importantly, with a hypothetical guanylyl cyclase (GC) center capable of that catalyzing the formation of cGMP from GTP (Wong et al., 2013; Domingos et al., 2015; Xu et al., 2018; Su et al., 2019). Our prediction was recently confirmed by others (Dias et al., 2019). Thus, we next focused on the catalytic activity of DGK4. Both cGMP and more strongly NO, inhibit DGK4 kinase activity, but NO did not affect the GC activity (Figure 2E). Mutations in the H-NOX center did not affect the kinase activity of DGK4 as both

H350L and Y379L dgk4 mutants were functional and inhibited by NO to comparable degree as the WT (Figure S5). While this result could nullify the hypothesis that the H-NOX center of *dgk4-1* works as an NO sensor, it must be considered that, while there is a reduction of intensity and slower recovery upon oxidation, there are still changes in the Soret band in the mutants, thus revealing some NO binding. Given that both the enzyme and the NO steady concentrations *in vivo* should be much lower (Prado et al., 2004), the range of physiological sensitization to NO may thus not be captured on the conditions of the enzymatic assays.

Another conceivable possibility that we cannot overrule at this point, is that NO-induced S-Nitrosylation is also taking place as reported for other kinases (Hu et al., 2017; Liu et al., 2017). DGK4 displays five S-Nitrosylation sites on C62, C138, C174, C260 and C334 (SNOSite, http://csb.cse.yzu.edu.tw/SNOSite/Prediction.html; Lee et al., 2011). Of these, C138 and C174 are in the kinase/GC domains but no S-Nitrosylation sites were predicted at the H-NOX center. Either way, since DGK4 is localized in the cytosolic region of the PT apex (Dias et al., 2019), our results are consistent with a signaling role for DGK4 in transducing NO-binding into lipid-, cGMP- or Ca^{2+}-dependent downstream responses. This conclusion is based on the fact that DGKs are known to convert DAG to PA that in turn is essential for PT growth (Pleskot et al., 2012; Potocký et al., 2014) and the mobilization of Ca^{2+} (Monteiro et al., 2005; Prado et al., 2008). Our biochemical data also show that, while the kinase activity of DGK4 is inhibited by cGMP, the GC activity of DGK4 is unaffected by NO, thus implying that the reduced NO response of *dgk4-1* PTs may be achieved primarily through the PA dependent lipid/Ca^{2+} signaling pathways rather than the activation of its GC

moonlighting center. While the existence of a cyclic nucleotide signaling paradigm in plants is controversial (Gehring and Turek, 2017; Świeżawska et al., 2018), cGMP has been shown to activate Ca^{2+} currents by the cyclic nucleotide-gated channel 18 (CNGC18) localized at the tip of PTs (Gao et al., 2016).

In summary, Figure 2F depicts a hypothetical mechanism for NO action in PTs. In this model, NO could have two distinct targets in DGK4: on one hand (i) NO modulates PT re-orientation responses by binding to the H-NOX center of DGK4, leading to a PA reduction; on the other hand (ii) NO inhibits the kinase and GC activities of DGK4 via S-Nitrosylation at C138 and/or C174. We hypothesize that differential kinetics of these mechanisms (H-NOX is predicted to occur much faster), different affinities of NO binding (defining different intervals of NO perception), and the role of cGMP (which we found to inhibit the kinase activity but is not affected by NO), could generate the sequential effects observed during our slowing/ re-orientation assays, and the lack of thereof in the mutant. The read-out of DGK-4 mediated reactions would be transduced into variations of PA, which is known to interplay with Ca^{2+} signaling, possibly triggering other downstream paths resulting in vesicular trafficking and/or actin dynamics alterations (Li et al., 1999; Chen et al., 2003). In agreement with this interpretation, *dgk4* PTs have recently been reported to exhibit altered mechanical properties with down-regulation of a cyclase associated protein, CAP1 which is involved in actin dynamics, and a general down-regulation of the phosphoinositide metabolism (Dias et al., 2019).

362 Importantly, slowing-down of PT is necessary for optimizing the perception of
363 chemical cues (Stewman et al., 2010) and this constitutes a plausible explanation for
364 the loss of chemotropic response in the mutant and contribute to the observed seed-set
365 reduction. As a fast-diffusible gas, NO is well suited to perform fine-tuning of rapid cell-
366 cell communications such as the pollen-stigma interactions (Prado et al., 2008; Feijó,
367 2010; Domingos et al., 2015) and we posit that DGK4 may be an important sensing
368 input mechanism of NO to regulate plant reproduction.

Supplementary information

Supplementary information contains five figures, two tables and supplementary references. Supplementary information available online at:

Competing interests

The authors declare no competing interest.

Author contributions

Conceptualization: C.G., J.F. ; Methodology: C.G., J.F., M.T.P., A.W., L.D., J.E.; Formal analysis: A.W., M.T.P., J.E.; Investigation: A.W., M.T.P., L.D., JF; Writing - original draft: A.W., C.G., L.D., J.E., M.T.P., J.F.; Writing - review & editing: A.W., C.G., L.D., J.E., M.T.P, J.F.; Supervision: C.G., L.D., J.F.; Project administration: C.G., L.D., J.F.; Funding acquisition: C.G., J.F.

Funding

This research was supported by the King Abdullah University of Science and Technology (C.G. lab) and National Science Foundation grants MCB-1616437 and MCB-1930165 (J.F. lab). A.W. is supported by the National Natural Science Foundation of China (Grant no. 31850410470) and the Zhejiang Provincial Natural Science Foundation of China (Grant no. LQ19C130001).

References

Aller, I., Rouhier, N. and Meyer, A.J. (2013). Development of roGFP2-derived redox probes for measurement of the glutathione redox potential in the cytosol of severely glutathione-deficient rml1 seedlings. *Front. Plant Sci.* **4**, 506, doi:10.3389/fpls.2013.00506.

Astier, J., Mounier, A., Santolini, J., Jeandroz, S. and Wendehenne, D. (2019). The evolution of nitric oxide signalling diverges between the animal and the green lineages. *J. Exp. Bot.* **erz088**, doi:10.1093/jxb/erz088.

Beltran, J., Kloss, B., Hosler, J. P., Geng, J., Liu, A., Modi, A., Dawson, J. H., Sono, M., Shumskaya, M., Ampomah-Dwamena, C., et al. (2015). Control of carotenoid biosynthesis through a heme-based cis-trans isomerase. *Nat. Chem. Biol.* **11**, 598-605.

Boavida, L.C., McCormick, S. (2007) Temperature as a determinant factor for increased and reproducible in vitro pollen germination in Arabidopsis thaliana. *Plant J.*, **52**(3), 570-582

Chen, C. Y., Cheung, A. Y., and Wu, H. M. (2003). Actin-depolymerizing factor mediates Rac/Rop GTPase-regulated pollen tube growth. *Plant Cell* **15**(1), 237-249.

Dai, Z., Farquhar, E. R., Arora, D. P. and Boon, E. M. (2012). Is histidine dissociation a critical component of the NO/H-NOX signaling mechanism? Insights from X-ray absorption spectroscopy. *Dalton Trans.* **41**, 7984-7993.

412 Dias, F. V. Serrazina, S., Vitorino, M., Marchese, D., Heilmann, I., Godinho, M.,
413 Rodrigues, M. and Malhó, R. (2019). A role for diacylglycerol kinase 4 in
414 signalling crosstalk during Arabidopsis pollen tube growth. *New Phytol.* **222**(3),
415 1434-1446.
416 Domingos, P., Prado, A.M., Wong, A., Gehring, C. and Feijo, J.A. (2015). Nitric oxide: a
417 multitasked signaling gas in plants. *Mol. Plant* **8**, 506-520.
418 Feijo, J. A. (2010). The mathematics of sexual attraction. *J. Biol.* **9**(3), 18,
419 doi:10.1186/jbiol233.
420 Gao, Q. F., Gu, L. L., Wang, H. Q., Fei, C. F., Fang, X., Hussain, J., Sun, S. J, Dong J.
421 Y., Liu, H. and Wang, Y. F. (2016). Cyclic nucleotide-gated channel 18 is an
422 essential Ca^{2+} channel in pollen tube tips for pollen tube guidance to ovules in
423 Arabidopsis. *Proc. Natl. Acad. Sci. U. S. A.* **113**, 3096-3101.
424 Gehring, C., and Turek, I. S. (2017). Cyclic nucleotide monophosphates and their
425 cyclases in plant signaling. *Front. Plant Sci.* **8**, 1704,
426 doi:10.3389/fpls.2017.01704.
427 He, J.M., Bai, X.L., Wang, R.B., Cao, B., and She, X.P. (2007). The involvement of nitric
428 oxide in ultraviolet-B-inhibited pollen germination and tube growth of Paulownia
429 tomentosa in vitro. *Physiol. Plant.* **131**(2), 273-282.
430 Ho, S. N., Hunt, H. D., Horton, R. M., Pullen, J. K. and Pease, L. R. (1989). Site-
431 directed mutagenesis by overlap extension using the polymerase chain reaction.
432 *Gene* **77**, 51-59.
433

Hu, J., Yang, H., Mu, J., Lu, T., Peng, J., Deng, X., Kong, Z., Bao, S., Cao, X., and Zuo, J. (2017). Nitric oxide regulates protein methylation during stress responses in plants. *Mol. Cell* **67**(4), 702-710.e4.

Lamattina, L., Garcia-Mata, C., Graziano, M. and Pagnussat, G. (2003). Nitric oxide: the versatility of an extensive signal molecule. *Annu. Rev. Plant. Biol.* **54**,109-136.

Lee, T. Y., Chen, Y. J., Lu, T. C., Huang, H. D., and Chen, Y. J. (2011). SNOSite: Exploiting maximal dependence decomposition to identify cysteine S-nitrosylation with substrate site specificity. *PLoS ONE* **6**, e21849, doi:10.1371/journal.pone.0021849.

Leon, J., Costa-Broseta, A. (2019) Present knowledge and controversies, deficiencies and misconceptions on nitric oxide synthesis, sensing and signaling in plants. *Plant Cell & Environ.* **43**(1), 1-15.

Li, H., Lin, Y., Heath, R. M., Zhu, M. X., and Yang, Z. (1999). Control of pollen tube tip growth by a Rop GTPase-dependent pathway that leads to tip-localized calcium influx. *Plant Cell* **11**(9), 1731-1142.

Liu, J. Z., Duan, J., Ni, M., Liu, Z., Qiu, W.L., Whitham, S.A., and Qian W. J. (2017). S-Nitrosylation inhibits the kinase activity of tomato phosphoinositide-dependent kinase 1 (PDK1). *J. Biol. Chem.* **292**(48), 19743-19751.

McInnis, S.M., Desikan, R., Hancock, J. T. and Hiscock, S. J. (2006). Production of reactive oxygen species and reactive nitrogen species by angiosperm stigmas and pollen: potential signalling crosstalk? *New Phytol.* **172**, 221-228.

Meijering, E., Jacob, M., Sarria, J. C., Steiner, P., Hirling, H. and Unser, M. (2004). Design and validation of a tool for neurite tracing and analysis in fluorescence microscopy images. *Cytometry A* **58**, 167-176.

Miraglia, E., De Angelis, F., Gazzano, E., Hassanpour, H., Bertagna, A., Aldieri, E., Revelli, A. and Ghigo, D. (2011). Nitric oxide stimulates human sperm motility via activation of the cyclic GMP/protein kinase G signaling pathway. *Reproduction* **141**, 47-54.

Monteiro, D., Liu, Q., Lisboa, S., Scherer, G. E. F., Quader, H. and Malhó, R. (2005). Phosphoinositides and phosphatidic acid regulate pollen tube growth and reorientation through modulation of $[Ca^{2+}]c$ and membrane secretion. *J. Exp. Bot.* **56**, 1665-1674.

Mori, T., Kuroiwa, H., Higashiyama, T. and Kuroiwa, T. (2006). GENERATIVE CELL SPECIFIC 1 is essential for angiosperm fertilization. *Nat. Cell Biol.* **8**, 64-71.

Pleskot, R., Pejchar, P., Bezvoda, R., Lichtscheidl, I. K., Wolters-Arts, M., Marc, J., Zarsky, V., and Potocký, M. (2012). Turnover of phosphatidic acid through distinct signaling pathways affects multiple aspects of pollen tube growth in tobacco. *Front. Plant Sci.* **3**, 54, doi:10.3389/fpls.2012.00054.

Potocký, M., Pleskot, R., Pejchar, P., Vitale, N., Kost, B. and Žárský, V. (2014). Live-cell imaging of phosphatidic acid dynamics in pollen tubes visualized by Spo20p-derived biosensor. *New Phytol.* **203**, 483-494.

Prado, A. M., Colaco, R., Moreno, N., Silva, A. C. and Feijo, J.A. (2008). Targeting of pollen tubes to ovules is dependent on nitric oxide (NO) signaling. *Mol. Plant* **1**, 703-714.

478 Prado, A. M., Porterfield, D. M. and Feijo, J.A. (2004). Nitric oxide is involved in growth
479 regulation and re-orientation of pollen tubes. *Development* **131**, 2707-2714.
480 Russwurm, M. and Koesling, D. (2004). NO activation of guanylyl cyclase. *EMBO J.* **23**,
481 4443-4450.
482 Schneider, C. A., Rasband, W. S. and Eliceiri, K. W. (2012). NIH Image to ImageJ: 25
483 years of image analysis. *Nat. Meth.* **9**, 671-675.
484 Sengoku, K., Kenichi, T., Toshiaki, Y., Yasuo, T., Toshinobu, M. and Mutsuo, I. (1998).
485 Effects of low concentrations of nitric oxide on the zona pellucida binding ability
486 of human spermatozoa. *Fertil. Steril.* **69**, 522-527.
487 Stewman, S. F., Jones-Rhoades, M., Bhimalapuram, P., Tchernookov, M., Preuss, D.
488 and Dinner, A. R. (2010). Mechanistic insights from a quantitative analysis of
489 pollen tube guidance. *BMC Plant Biol.* **10**, 32, doi:10.1186/1471-2229-10-32.
490 Su, B., Qian, Z., Li, T., Zhou, Y., and Wong, A. (2019). PlantMP: a database for
491 moonlighting plant proteins. *Database* **2019**(2019), baz050,
492 doi:10.1093/database/baz050.
493 Świeżawska, B., Duszyn, M., Jaworski, K., and Szmidt-Jaworska, A. Downstream
494 targets of cyclic nucleotides in plants. *Front. Plant Sci.* **9**, 1428,
495 doi:10.3389/fpls.2018.01428.
496 Walker, F. A., Ribeiro, J. M. and Montfort, W. R. (1999). Novel nitric oxide-liberating
497 heme proteins from the saliva of bloodsucking insects. *Met. Ions Biol. Syst.* **36**,
498 621-663.
499 Wang, Y., Chen, T., Zhang, C., Hao, H., Liu, P., Zheng, M., Baluška, F., Šamaj, J. and
500 Lin, J. (2009). Nitric oxide modulates the influx of extracellular Ca^{2+} and actin

filament organization during cell wall construction in Pinus bungeana pollen tubes. *New Phytol.* **182**, 851-862.

Wang, Y. H., Li, X. C., Zhu-Ge, Q., Jiang, X., Wang, W. D., Fang, W. P., Chen, X. and Li, X. H. (2012). Nitric oxide participates in cold-inhibited Camellia sinensis pollen germination and tube growth partly via cGMP in vitro. *PLoS One* **7**, e52436, doi:10.1371/journal.pone.0052436.

Wendehenne, D., Pugin, A., Klessig, D. F. and Durner, J. (2001). Nitric oxide: comparative synthesis and signaling in animal and plant cells. *Trends Plant Sci.* **6,** 177-183.

Wong, A., Donaldson, L., and Gehring, C. (2013). The enzymatic activity of Arabidopsis diacylglycerol kinase 4 (ATDGK4) is regulated by nitric oxide. 16th International Workshop on Plant Membrane Biology. https://f1000research.com/posters/1093019.

Wong, A., Tian, X., Gehring, C., and Marondedze, C. (2018). Discovery of novel functional centers with rationally designed amino acid motifs. *Comput. Struct. Biotechnol. J.* **16**, 70-76, doi:10.1016/j.csbj.2018.02.007.

Xu, N., Fu, D., Li, S., Wang, Y., and Wong, A. (2018). GCPred: a web tool for guanylyl cyclase functional center prediction from amino acid sequence. *Bioinformatics* **34**(12), 2134-2135.

Zarban, R., Vogler, M., Wong, A., Eppinger, J., Al-Babili, S., and Gehring, C. (2019). Discovery of a nitric oxide-responsive protein in Arabidopsis thaliana. *Molecules* **24**(15), E2691, doi:10.3390/molecules24152691.

Figure 1

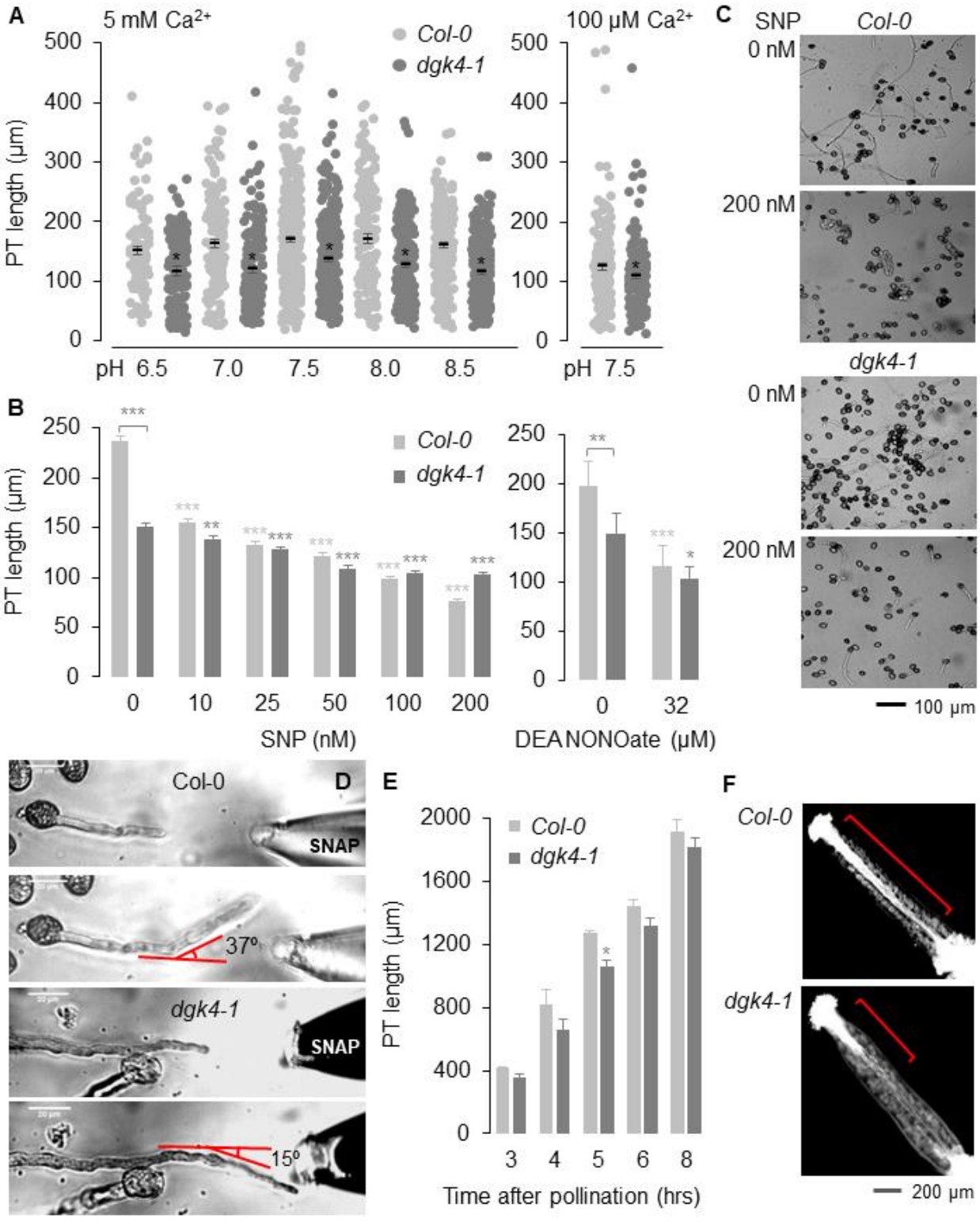
A
5 mM Ca2+
100 µM Ca2+
Col-0
dgk4-1
PT length (µm)
pH 6.5
7.0
7.5
8.0
8.5
pH 7.5
B
PT length (µm)
SNP (nM)
DEANONOate (µM)
C
SNP
Col-0
0 nM
200 nM
dgk4-1
100 µm
D
Col-0
SNAP
37º
dgk4-1
15º
E
PT length (µm)
Time after pollination (hrs)
F
Col-0
dgk4-1
200 µm

Figure 1. *dgk4-1* PT has reduced growth and NO-dependent responses

(**A**) *dgk4-1* PT growth is slower than that of *Col-0* consistent across a range of pH (6.5-8.5) and in both optimal (5 mM) (left) and reduced (100 µM) Ca^{2+} (right) media. Error bars represent s.e.m. ($n > 100$). * = $P < 0.05$ compared to PT length of *Col-0*. (**B**) NO-dependent inhibition of *dgk4-1* PT growth is reduced compared to that of *Col-0*. NO was provided by SNP or DEA NONOate. (**C**) Representative images of *dgk4-1* and *Col-0* PTs with and without NO. Error bars represent s.e.m. ($n > 150$). * = $P < 0.05$, ** = $P < 0.005$ and *** = $P < 0.0005$ compared to PT length of untreated sample. (**D**) A representative image of the response of a growing *Col-0* PT bending away from an agarified NO glass probe containing SNAP (10 mM) at a sharper angle than *dgk4-1* (see also Figure S3). (**E**) PT growth in the pistil of *dgk4-1* is slowed compared to *Col-0* with (**F**) the representative pistil image at 5 hours post-fertilization showing a higher density of longer *Col-0* PTs. Error bars represent s.e.m. ($n > 3$). * = $P < 0.05$ compared to PT length of *Col-0*.

Figure 2

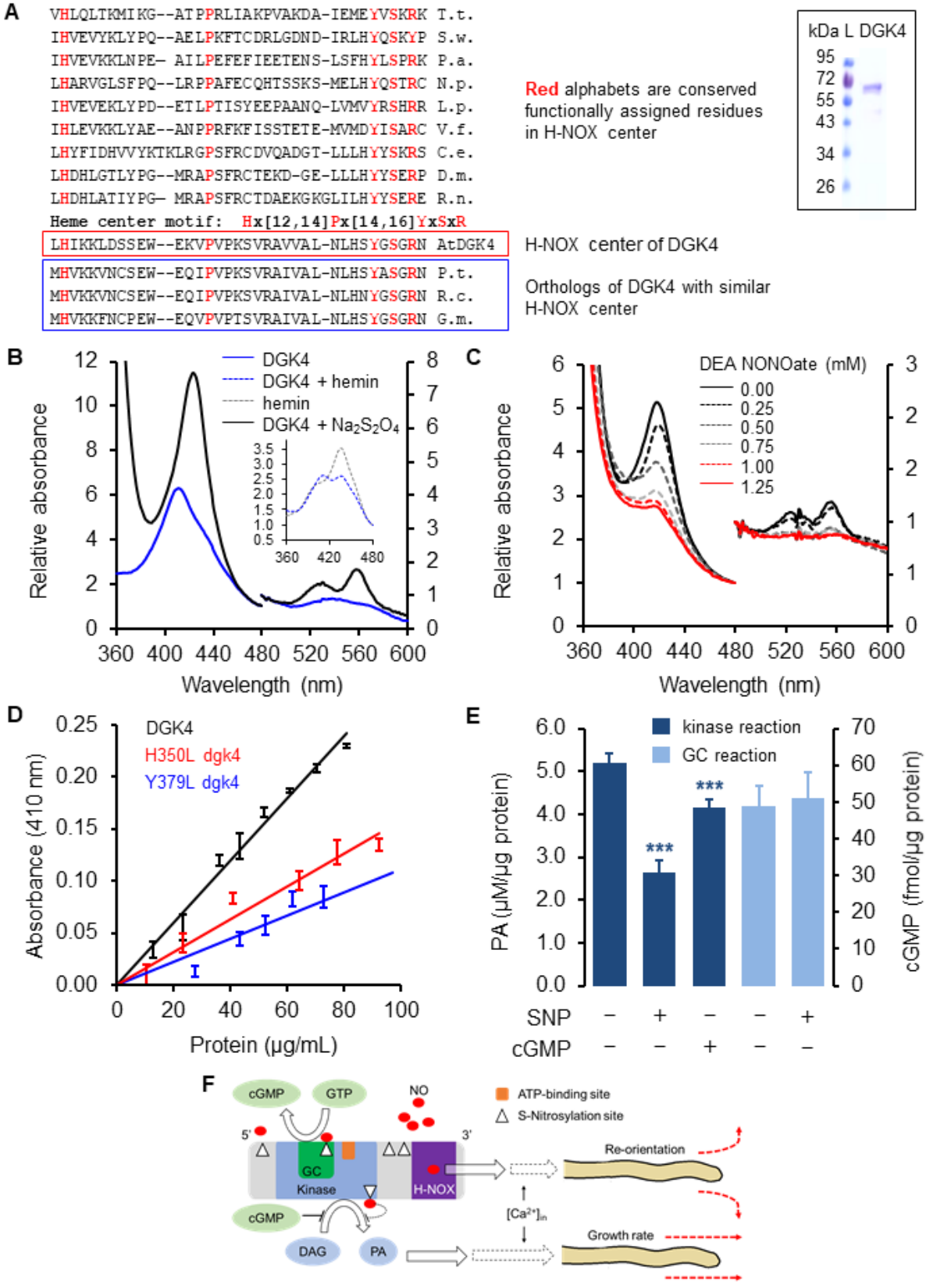
A
VHLQLTKMIKG--ATPPRLIAKPVAKDA-IEMEYVSKRK T.t.
IHVEVYKLYPQ--AELPKFTCDRLGDND-IRLHYQSKYP S.w.
IHVEVKKLNPE- AILPEFEFIEETENS-LSFHYLSPRK P.a.
LHARVGLSFPQ--LRPPAFECQHTSSKS-MELHYQSTRC N.p.
IHVEVEKLYPD--ETLPTISYEEPAANQ-LVMVYRSHRR L.p.
IHLEVKKLYAE--ANPPRFKFISSTETE-MVMDYISARC V.f.
LHYFIDHVVYKTKLRGPSFRCDVQADGT-LLLHYYSKRS C.e.
LHDHLGTLYPG--MRAPSFRCTEKD-GE-LLLHYYSERP D.m.
LHDHLATIYPG- MRAPSFRCTDAEKGKGLILHYYSERE R.n.
Heme center motif: Hx[12,14]Px[14,16]YxSxR
LHIKKLDSSEW--EKVPVPKSVRAVVAL-NLHSYGSGRN AtDGK4
MHVKKVNCSEW--EQIPVPKSVRAIVAL-NLHSYASGRN P.t.
MHVKKVNCSEW--EQIPVPKSVRAIVAL-NLHNYGSGRN R.c.
MHVKKFNCPEW--EQVPVPTSVRAIVAL-NLHSYGSGRN G.m.
Red alphabets are conserved functionally assigned residues in H-NOX center
H-NOX center of DGK4
Orthologs of DGK4 with similar H-NOX center
kDa L DGK4
95
72
55
43
34
26
B
Relative absorbance
Wavelength (nm)
DGK4
DGK4 + hemin
hemin
DGK4 + Na2S2O4
C
Relative absorbance
Wavelength (nm)
DEA NONOate (mM)
0.00
0.25
0.50
0.75
1.00
1.25
D
Absorbance (410 nm)
Protein (μg/mL)
DGK4
H350L dgk4
Y379L dgk4
E
PA (μM/μg protein)
cGMP (fmol/μg protein)
kinase reaction
GC reaction
***
***
SNP
cGMP
F
cGMP
GTP
NO
ATP-binding site
S-Nitrosylation site
5'
3'
GC
Kinase
H-NOX
Re-orientation
[Ca2+]in
cGMP
DAG
PA
Growth rate

Figure 2. DGK4 has NO-responsive spectral and catalytic activity

(**A**) The region H350 to R383 in DGK4 contains amino acid residues of annotated heme centers of gas-responsive proteins as shown in the alignment of *Thermoanaurobacter tengcongensis* (T.t.; GI: 3566245696), *Shewanella woodyi* (S.w.; Gl: 169812443), *Pseudoalteromonas atlantica* (P.a.; GI: 109700134), *Nostoc punctiforme* (N.p.; GI: 126031328), *Legionella pneumophila* (L.p.; GI: 52841290), *Vibrio fischeri* (V.f.; GI: 59713254), *Caenorhabditis elegans* (C.e.; GI: 52782806), *Drosophila melanogaster* (D.m.; GI: 861203), *Rattus norvegicus* (R.n.; GI:27127318), *Homo sapiens* (H.s.; GI: 2746083), *Arabidopsis thaliana* (A.t.; GI: 145359366), *Populus trichocarpa* (P.t.; GI: 224143809), *Ricinus communis* (R.c.; GI: 255581896) and *Glycine max* (G.m.; GI: 356567686) hemoproteins. Inset: Recombinant DGK4 was generated and purified according to procedures described in Materials and Methods. (**B**) DGK4 (inset) contains a cytochrome b_5 type heme center as indicated by the electronic absorption spectra in the ferric and ferrous state (Table S1). (**C**) UV-vis characterization of recombinant DGK4 reveals that NO attenuates the Soret peak of the ferrous heme center in a concentration dependent manner. (**D**) The H350L and Y379L dgk4 mutants have reduced heme binding. At 80 µg of protein, H350L and Y379L dgk4 have Soret peaks that are 0.5- and 0.3-fold of DGK4 (n = 3; n = independent experiments). (**E**), The kinase activity of DGK4 was reduced in the presence of SNP (1 mM) or cGMP (1 mM) but the GC activity was unaffected by SNP (1 mM) (n = 3; n = independent experiments). *** = $P < 0.0005$ compared to activity of DGK4 with no SNP or cGMP. (**F**) A model of DGK4 signaling roles in mediating NO-dependent PT growth and re-orientation responses. NO modulates PT re-orientation responses by binding to the H-

NOX center and/or inhibiting the kinase activity possibly via S-Nitrosylation at C138 and/or C174, yielding reduced PA which in turns, modulates cytosolic Ca^{2+}. Differential kinetics of these mechanisms, different affinities of NO binding and the role of cGMP inhibiting the kinase activity but unaffected by NO, could generate the sequential effects on PT retardation, re-orientation and growth resumption responses.

Supplementary information

Figure S1

Characterization of *dgk4* T-DNA insertion mutant plants

Figure S2

Homozygous *dgk4-2* PT has slower growth rate and reduced NO-dependent growth response

Figure S3

Variability of PT growth responses to SNP, NO-generating pipette sources

Figure S4

DGK4 harboring point mutation at the H-NOX-like center yields spectral behavior similar to WT

Figure S5

Kinase activities of DGK4 and mutant dgk4 harboring point mutations at the H-NOX-like center were inhibited by NO

Table S1

UV-Vis spectroscopic data of selected heme proteins

Table S2

Primers for cloning of *DGK4* and characterization of *dgk4-1* and *dgk4-2* plants

Movie S1

PT re-orientation responses of *Col-0* and *dgk4-1* to NO

Supplementary references

Figure S1. Characterization of *dgk4* T-DNA insertion mutant plants

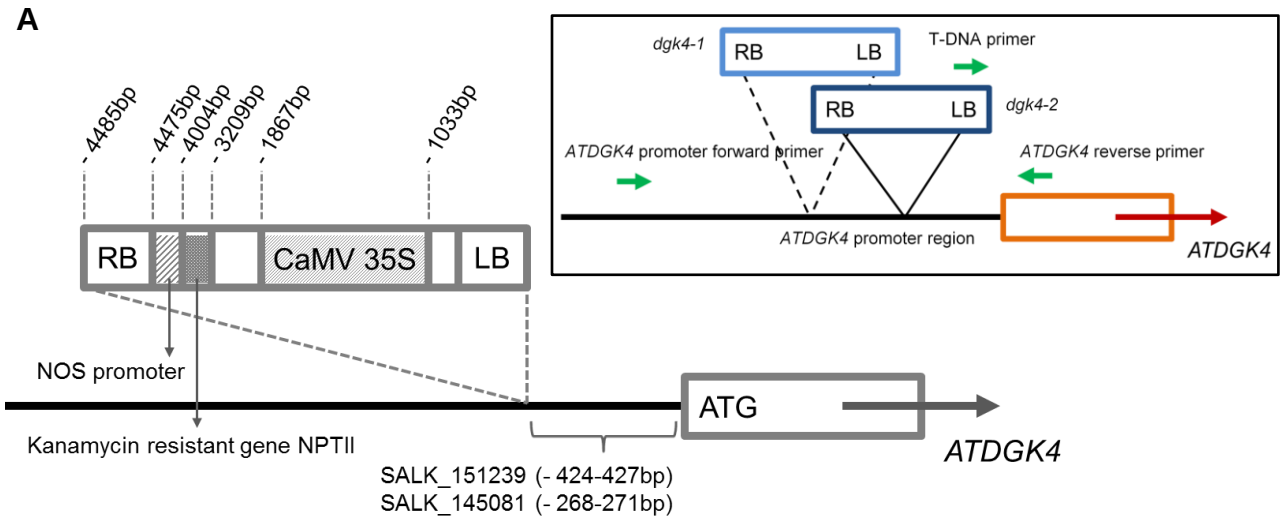

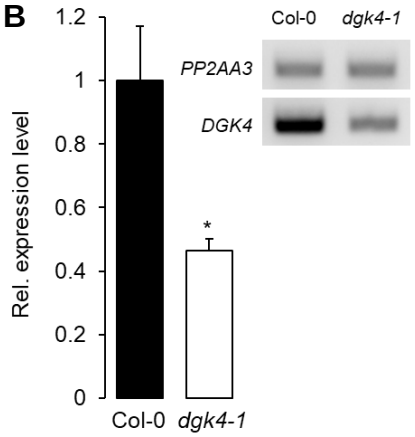

Legend:

SALK_151239 is designated as *dgk4-1*

SALK_145081 is designated as *dgk4-2*

(**A**) Schematic view of T-DNA insertion sites of *dgk4* mutants. Location and content of SALK T-DNA insertions are labelled. LB and RB indicate Left Border and Right Border of the T-DNA respectively. Inset: Green arrows indicate the position and direction of primers (see Table S2) used in RT-PCR to determine *DGK4* expression levels. (**B**) *dgk4-1* pollen has reduced *DGK4* mRNA levels as estimated by semi-quantitative RT-PCR. * = $P < 0.05$ compared to *DGK4* mRNA levels of *Col-0* pollen and gel pictures are representative of three independently derived biological replicates.

Figure S2. Homozygous *dgk4-2* PT has slower growth rate and reduced NO-dependent growth response

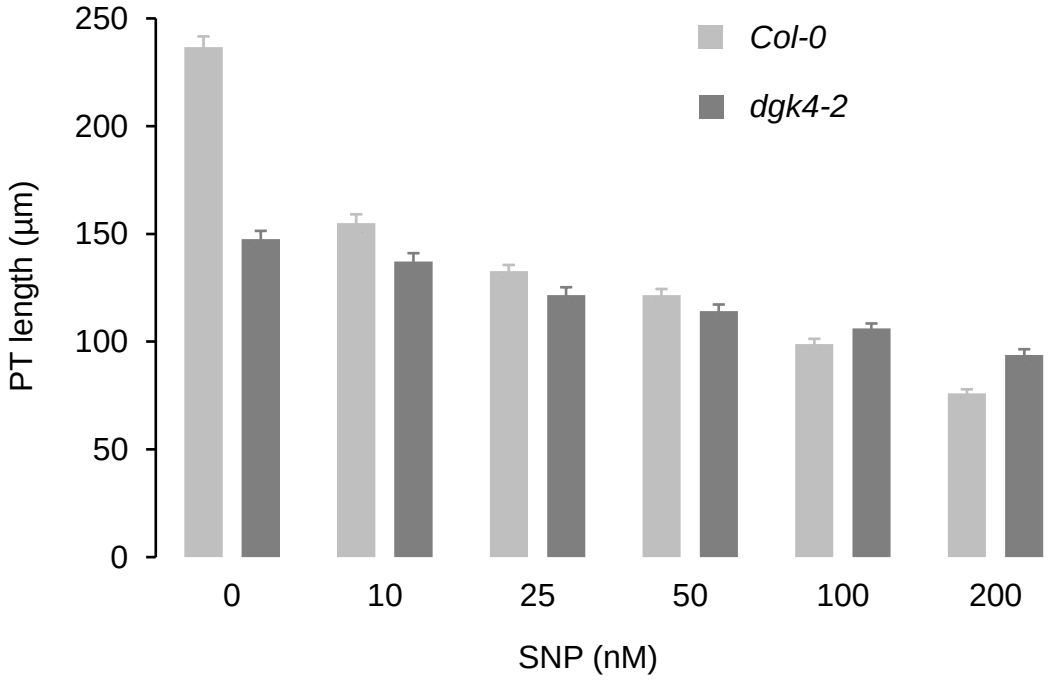

NO-dependent inhibition of *dgk4-2* PT growth is reduced compared to that of *Col-0*. NO was provided by either SNP. *In vitro* pollen germination was performed as detailed previously (Prado et al., 2004; Prado et al., 2008) and PT length was analyzed by capturing images covering the entire growth area of the culture dish that is mounted on an automated stage using the Nikon Eclipse TE2000-S inverted microscope equipped with a Hamamatsu Flash28s CMOS camera. The PT lengths were then measured using NeuronJ (Meijering et al., 2004). Error bars represent s.e.m. (n > 150).

Figure S3. Variability of PT growth responses to SNP, NO-generating pipette sources

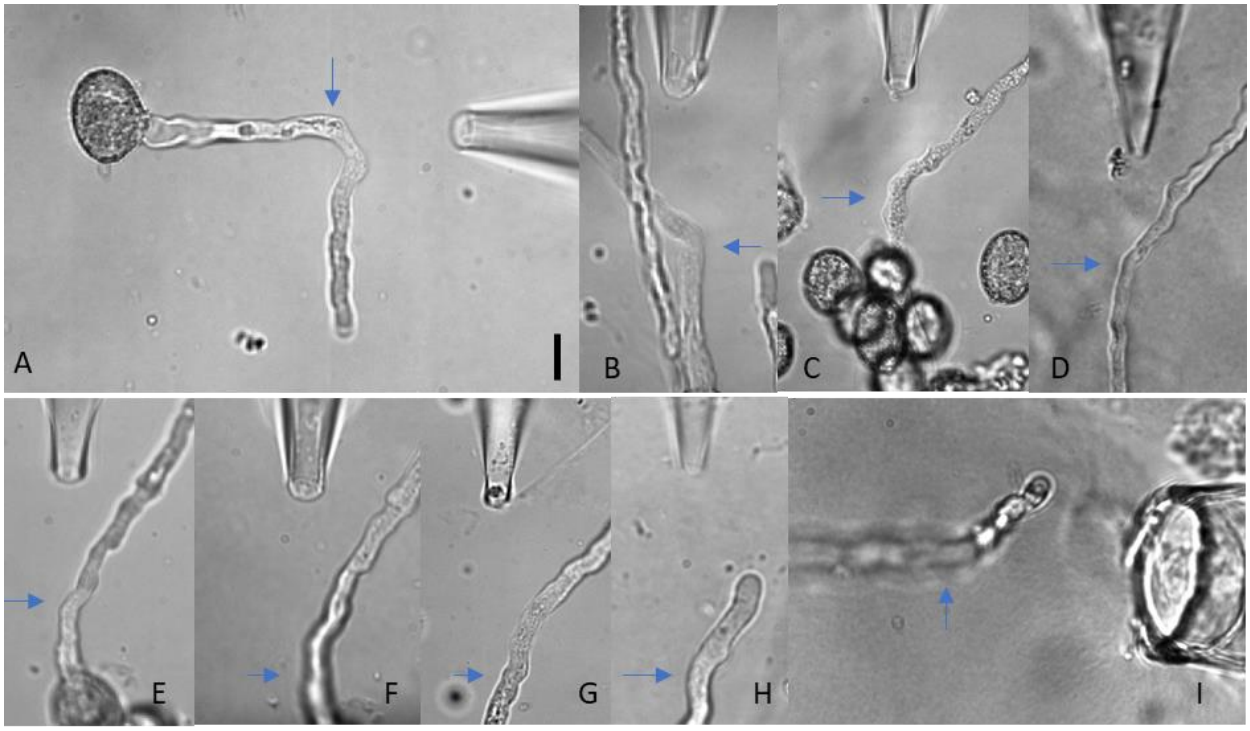

Top row: WT, bottom row: *dgk4-1.* Blue arrows represent the time point of the tip when the sources were positioned. Individual *Col-0* and *dgk4-1* PT bending angles were 37°, 35°, 28°, 28°, 90°, 48°, 29°, 69°, 44° and 50°, and 15°, 9°, 21°, 14°, 33°, 21°, 31°, 32°, 26° and 27° respectively. While a lone 90º orientation was observed for WT (**A**), most tubes show angles around 35-40º (**B**, **C** and **D**). They all showed clear, elbow-like, point of inflections when approaching the critical NO concentration to produce a response (see also Figure 1D, *Col-0*). This elbow turns were also observed in lily (Prado et al., 2004) and correspond to a slowdown/halt of the growth rate, followed by turning of the PT. In contrast, *dgk4-1* PTs always show smoother or softer turns around 20º (**E**, **F**, **G** and **H**), usually without much impact on the growth rate. On trying to push the boundary of how

much *dgk4-1* PTs can turn, we made experiments with pipettes more than twice the tip diameter and with ca. twice the concentration of SNP. In these conditions, majority of the *dgk4-1* PTs stopped growing with just a few growing at very slow rates but with obvious sick growth features and with rare re-directioning events. Even under these extreme conditions (**I**) the observed turning angle was below the average angle observed for WT and with no elbow-like turn. Bar represents 10 µm. The PT NO-dependent re-orientation response was monitored by real-time imaging and analyzed according to details in Materials and Methods.

Figure S4. DGK4 harboring point mutation at the H-NOX-like center yields spectral behavior similar to WT

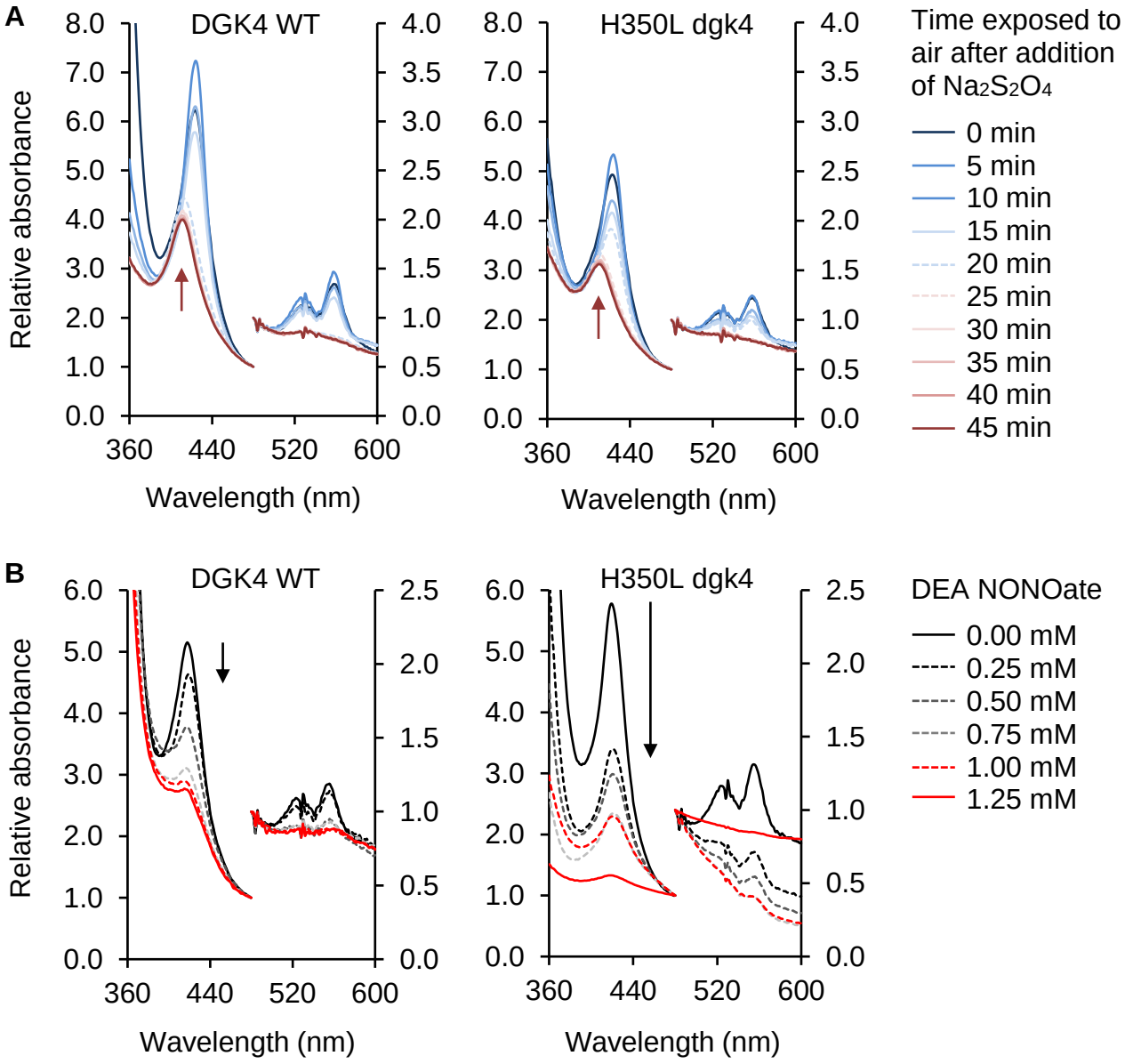

(**A**) UV-vis characterization reveals that the Soret peaks (410 nm) of 80 µg DGK4 WT and H350L dgk4 mutant proteins were both red-shifted to 424 nm accompanied by the emergence of distinct α (558 nm) and β (526 nm) bands when reduced with sodium dithionite. The oxidized Soret peaks (410 nm) (red arrows) of both DGK4 WT and H350L

dgk4 mutant were fully recovered after 20 and 25 min of exposure to air respectively. (**B**) Addition of DEA NONOate to reduced DGK4 and H350L dgk4 attenuates the Soret absorption (424 nm) in a concentration dependent manner where the Soret, *β*- and *α*-peaks vanish with increasing concentration of the NO donor. H350L dgk4 mutant recorded a much larger decrease in reduced Soret bands than that observed with DGK4 WT at low NO donor concentration (0.25 mM DEA NONOate) (black arrows) while also requiring a slightly longer time (~ 5 min more than DGK4 WT) (red arrows) to recover its oxidized Soret peak (410 nm) when exposed to air.

Figure S5. Kinase activities of DGK4 and mutant dgk4 harboring point mutations at the H-NOX-like center were inhibited by NO

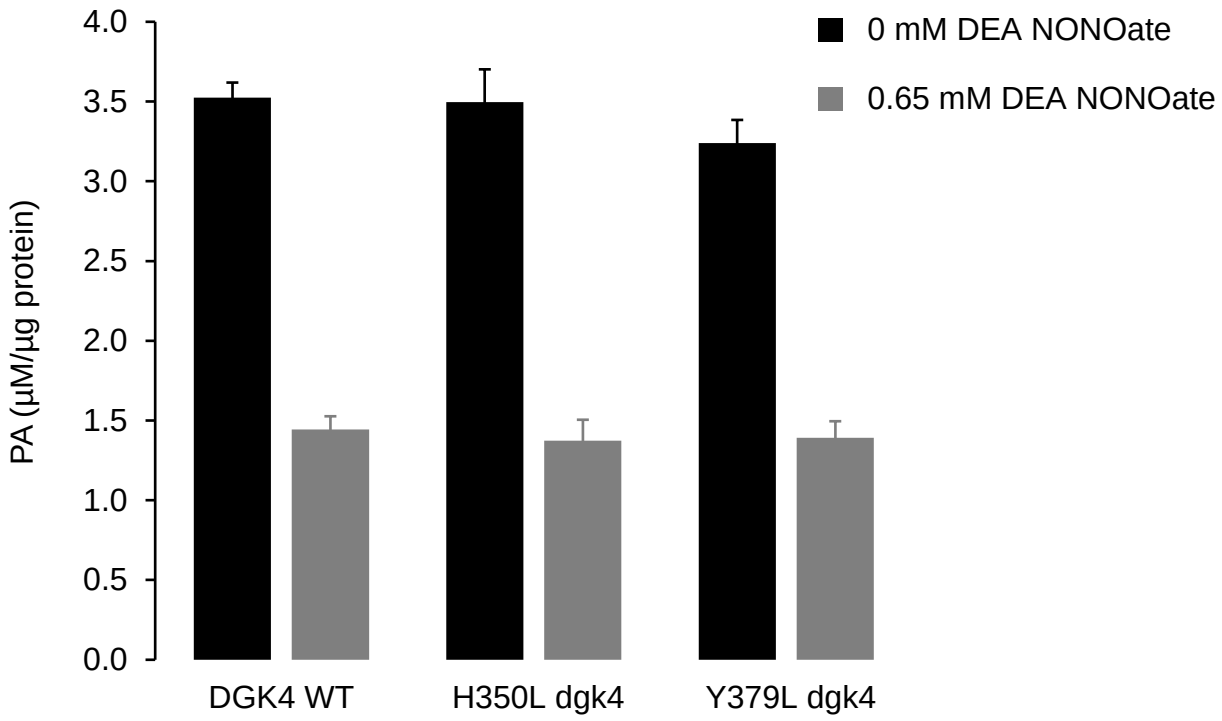

The kinase activities of dgk4 mutants H350L and Y379L were unaffected by the point mutations at the H-NOX-like center and were inhibited by NO to comparable degree as the WT. Kinase assay was done in reaction mixtures containing 40 mM Bis-Tris (pH 7.5), 5 mM $MgCl_2$, 0.1 mM EDTA, 1 mM spermine, 0.5 mM dithiothreitol, 1 mM sodium deoxycholate, 0.02% (v/v) Triton X-100, 500 µM 1,2-DOG and 1 mM ATP, with or without 0.65 mM DEA NONOate (see Materials and Methods for details). Black solid bars represent kinase reactions performed in the absence of NO while grey solid bars represent kinase reactions performed in the presence of NO (*n* = 6).

Table S1. UV-Vis spectroscopic data of selected heme proteins

	Soret / β / α ; max. absorption / nm			Source
Protein (*sp.*)	ferric	ferrous	ferrous-NO	
DGK4 (*At*)	410 / α + β 534	424 / 526 / 558	418 / - / -	This work
H-NOX (*So*)	403 / - / -	430 / α + β 560	399 / 543 / 572	Herzik et al., 2014
Cyt b5 (*Gl*)	411 / α + β 532	423 / 526 / 558		Alam et al., 2012
Z-ISO (*At*)	414 / α + β 531	414 / 529 / 559		Beltran et al., 2015

Legend: *At*: *Arabidopsis thaliana, So: Shiwanella oneidensis, Gl: Giardia lamblia.*

Table S2. Primers for cloning of *DGK4* and characterization of *dgk4-1* and *dgk4-2* plants

Primer name	Sequence (5’ – 3’)
***DGK4* cloning**	
DGK4 F	ATGGAATCACCGTCGATTGG
DGK4 R	TCAATCTCCTTTGACGACCAA
DGK4 H-L F	TTATGACATTGCTTATAAAAAAGTTGG
DGK4 H-L R	CAACTTTTTTATAAGCAATGTCATAAA
DGK4 Y-L F	ATCTACATAGCTTAGGAAGTGGAAGAA
DGK4 Y-L R	TCTTCCACTTCCTAAGCTATGTAGATT
Screening for homozygous *dgk4-1* and *dgk4-2* plants	
DGK4 promoter forward	TGTTTCTGACATCTGAGAACTTTT
DGK4 reverse	GATTGCATTCTTCGTAAAGACG
T-DNA	GTTCACGTAGTGGGCCATCG
Expression of *DGK4*	
DGK4 qPCR forward	CGTCGATTGGTGATTCATTG
DGK4 qPCR reverse	TTGCAATGCGGAGATATTGA
PP2AA3 qPCR forward	GCGGTTGTGGAGAACATGATACG
PP2AA3 qPCR reverse	GAACCAAACACAATTCGTTGCTG

Note: The underlined nucleotides incorporate the mutations changing histidine or tyrosine residues at positions 350 and 379 to leucine.

Movie S1. PT re-orientation responses of *Col-0* and *dgk4-1* to NO

Movie file attached separately.

Supplementary references

1. Prado, A. M., Colaco, R., Moreno, N., Silva, A. C. and Feijo, J.A. (2008). Targeting of pollen tubes to ovules is dependent on nitric oxide (NO) signaling. *Mol. Plant* **1**, 703-714.
2. Prado, A. M., Porterfield, D. M. and Feijo, J.A. (2004). Nitric oxide is involved in growth regulation and re-orientation of pollen tubes. *Development* **131**, 2707-2714.
3. Meijering, E., Jacob, M., Sarria, J. C., Steiner, P., Hirling, H. and Unser, M. (2004). Design and validation of a tool for neurite tracing and analysis in fluorescence microscopy images. *Cytometry A* **58**, 167-176.
4. Herzik, M. A., Jonnalagadda, R., Kuriyan, J. and Marletta, M. A. (2014). Structural insights into the role of iron–histidine bond cleavage in nitric oxide-induced activation of H-NOX gas sensor proteins. *Proc. Natl. Acad. Sci. U.S.A.* **111**, E4156-E4164.
5. Alam, S., Yee, J., Couture, M., Takayama, S. J., Tseng, W. H., Mauk, A. G. and Rafferty, S. (2012). Cytochrome b5 from Giardia lamblia. *Metallomics* **4**, 1255-1261.

6. Beltran, J., Kloss, B., Hosler, J. P., Geng, J., Liu, A., Modi, A., Dawson, J. H., Sono, M., Shumskaya, M., Ampomah-Dwamena, C. et al. (2015). Control of carotenoid biosynthesis through a heme-based cis-trans isomerase. *Nat. Chem. Biol.* **11**, 598-605.